

Shadow bands observed during the total solar eclipse of 4 December 2002, by high-resolution imaging

Szymon Gladysz^{a,*}, Michael Redfern^a, Barrie W. Jones^b

^a*Experimental Physics Department, National University of Ireland, Galway, Ireland*

^b*Physics and Astronomy Department, The Open University, Milton Keynes MK7 6AA, UK*

Received 30 March 2004; received in revised form 16 December 2004; accepted 26 February 2005
Available online 19 May 2005

Abstract

This paper presents results of a comparison between the characteristics of shadow bands recorded during the total solar eclipse of 4 December 2002 in Botswana, and the theory of Codona (Codona, 1986, *Astronomy and Astrophysics* 164, 415–427). For the first time the analysis was based on images of the phenomenon and not photometric data. Thanks to this, use was made of high spatial resolution and detailed plots of power spectra were obtained. The plots' shapes are in excellent agreement with those predicted by theory. From them, the height of the scattering layer producing shadow bands was inferred.

© 2005 Elsevier Ltd. All rights reserved.

Keywords: Eclipses; Scintillation; Seeing

1. Introduction

Shadow bands appear just before and just after the total phase of solar eclipses. They are roughly linear patterns moving across the ground with typical speeds of a few metres per second (m s^{-1}) in the direction perpendicular to their elongation. They align parallel to the tangent to the centre of the solar crescent (Marschall et al., 1984). When the observer is not directly on the centre of the path of totality, the crescent will be rotating, thus the direction of the shadow bands movement will also rotate with it. It has been observed that shadow band spacing decreases and their contrast increases as totality approaches (Codona, 1986).

Codona proposed a theory to explain the phenomenon. He suggested that shadow bands are a scintillation effect: the solar crescent, which has a non-uniform

brightness distribution, illuminates density inhomogeneities in the Earth's atmosphere. These have different refractive indices at any instant in time. The crescent is treated as an infinitely distant, extended, incoherent line source. The plane wave from each element of the line source encounters refractive index inhomogeneities and produces a speckle pattern on the ground. The superposition of the patterns from all of the elements of the line source tends to produce linear features in a preferred direction determined by the overall shape of the crescent. Codona derived a formula for the spatial power spectrum of the shadow bands' intensity fluctuations, which displays three characteristic spatial frequencies. Each of them is controlled by the height of a thin, weakly scattering atmospheric layer. Because of the low contrast of the phenomenon it was until now studied photometrically, with an array of a few photodiodes, and approximate laws for the temporal characteristics were applied (the assumption was Taylor's hypothesis of 'frozen' turbulence) (Marschall et al., 1984, Jones, 1994,

*Corresponding author.

E-mail address: szymon.gladysz@nuigalway.ie (S. Gladysz).

Table 1
Local circumstances of the eclipse

Mid-totality (UT)	t_d (s)	Solar azimuth (deg.)	Solar altitude (deg.)	R_s (arcsec)	r	Ω (arcsec s ⁻¹)
06:10	73	104	34.6	973.7	1.0180	0.480

Nomenclature: t_d , eclipse duration; R_s , solar radius (mid-eclipse); r , lunar angular radius/solar angular radius (local); Ω , angular velocity of the Moon relative to the Sun.

1996, 1999). We present the first results of shadow band studies based on images and interpreted using Codona's theory. This means, in effect, that we had hundreds of thousands of detectors (represented by pixels on the pictures) running at the same time. We make use of explicit formulas in the spatial domain in order to determine the height of the scattering layer.

2. Obtaining the data

Shadow bands were recorded during the total solar eclipse of 4 December 2002 in Botswana at longitude 25.5°E and latitude 19.1°S, within a kilometre of the centre of totality. Table 1 gives the data for our local circumstances (from Espenak and Anderson, 2001).

The imaging system consisted of a white, diffusely reflective screen, 1000 mm wide and 800 mm tall (made of four segments), positioned at 55.4° angle from the ground so that the surface was perpendicular to the line of sight to the eclipsed Sun. A digital video recorder on a tripod was mounted approximately 2 m in front of it. The recorder was a Panasonic NV-MX500 using miniDV format. The aperture was locked fully open at $f/2.85$, and the exposure time was 1 ms so that the phenomenon was 'frozen'. The recorder captured 25 non-interlaced frames per second (fps). In order to increase sensitivity, the digital video conversion gain was increased by 18 dB, thus electronic noise was introduced. This noise was subtracted during offline data processing as described later. MiniDV is a compressed format—it employs a lossy algorithm for video compression: the Discrete Cosine Transform. DCT concentrates most energy in the low-frequency zone; the coefficients of the higher frequencies are small—small enough to be neglected with little visible distortion. The frames were extracted from the recording and saved as TIFF (uncompressed format) images, 720 × 576 pixels, on a PC. The colour system was RGB, and the bit depth was 24 bits (8 bits per band).

The bands were also observed visually. They were weak and disorganized and resembled the surface of boiling water rather than linear patterns.

Weather maps were used to deduce the wind's speed and direction. In the lower troposphere, where the bands

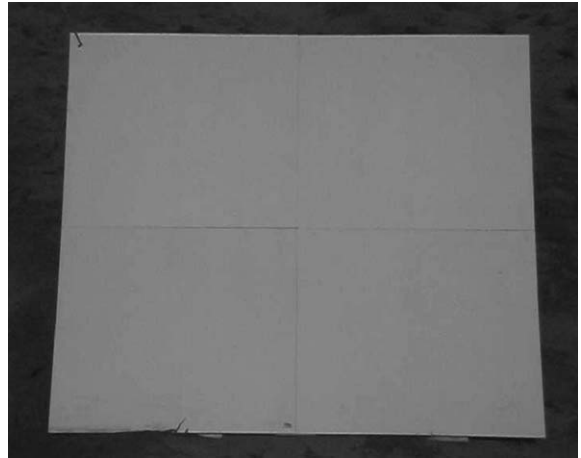


Fig. 1. A typical image of the screen, 50 s before totality. Shadow bands are of extremely low contrast in this image. They cannot be seen in a single frame. Visual perception is much better with a movie, because of the image processing capabilities of the eye/brain.

form, the winds were from the east–south–east (azimuth about 110°), at a speed of 2–4 m s⁻¹.

3. Image processing

All operations described in what follows were performed using the IDL programming language and a personal computer:

1. Because we could not place the camera between the source and the screen there was a certain amount of perspective elongation that had to be removed from the images (Fig. 1). Perspective transformation arises if a planar object is viewed from a fixed point in space (Glasbey and Mardia, 1998):

$$u = \frac{a_{10}x + a_{01}y + a_{00}}{c_{10}x + c_{01}y + 1}, \quad v = \frac{b_{10}x + b_{01}y + b_{00}}{c_{10}x + c_{01}y + 1},$$

where x, y are the coordinates of a point in the object plane, and u, v are the coordinates of the same point in the image plane. The inverse transformation

$(u,v) \rightarrow (x,y)$ was applied to every image using the reciprocal formulae. The eight parameters (a_{10} , a_{01} , a_{00} , b_{10} , b_{01} , b_{00} , c_{10} and c_{01}) were found using known positions of the four corners of the screen before and after the transformation. This meant solving a system of eight linear equations with eight unknowns. Bubic interpolation was used for image scaling.

2. Subsequently images were flat-fielded using ensemble-average as a flat-field. This is a simple variant of a technique proposed by Lindler et al. (1993) for Hubble Space Telescope's Faint Object Spectrograph and usually referred to as 'superflats'. The general decreasing (increasing) trend in overall brightness before (after) totality was removed by normalization. This produced images with the same intensity level as the first (last) image in the sequence. Background around the screen was cropped. This yielded images with dimensions 620×490 pixels.
3. The RGB colour scheme was transformed into the Hue, Luminance and Saturation (HLS) system and only the L-band corresponding to intensity was used throughout further analysis. The intensity values on the screen were in a very small range (30, 40 values on a 0–255 scale). With the single L-band we were able to widen this range without introducing chromatic errors. We decided to enhance the contrast by applying Gaussian curve fitting algorithm to the histogram of intensity and this way determining the range that had to be widened (Fig. 2). Afterwards we transformed each value in the histogram to a corresponding new 'bin' between 0 and 255. Thanks to this we achieved values that covered the whole scale. The dynamic range was narrowed down to 8 bits but since we limited the analysis to monochromatic phenomena this had no effect on further work.

4. Results

Two batches of 1480 images (59.2 s) before and after totality were used for further analysis. Immediately after third contact there was not enough light for the recorder's auto-focus mechanism to bring image into focus. That is why approximately 16 s of recording time after totality was removed from the analyzed data. For the two segments the *rms* value of intensity fluctuations (for a uniform part of one image) divided by the background irradiance was computed every 25 images (1 s). This was assumed to be a good measure of the shadow bands' contrast (Jones, 1996, 1999). Fig. 3 shows the results.

On two previous eclipses, Jones (1996, 1999) found shadow bands with contrasts in the range 0.2–0.9%. On 4 December 2002 the shadows were very weak and *rms* values had a maximum around 0.35%. What is striking

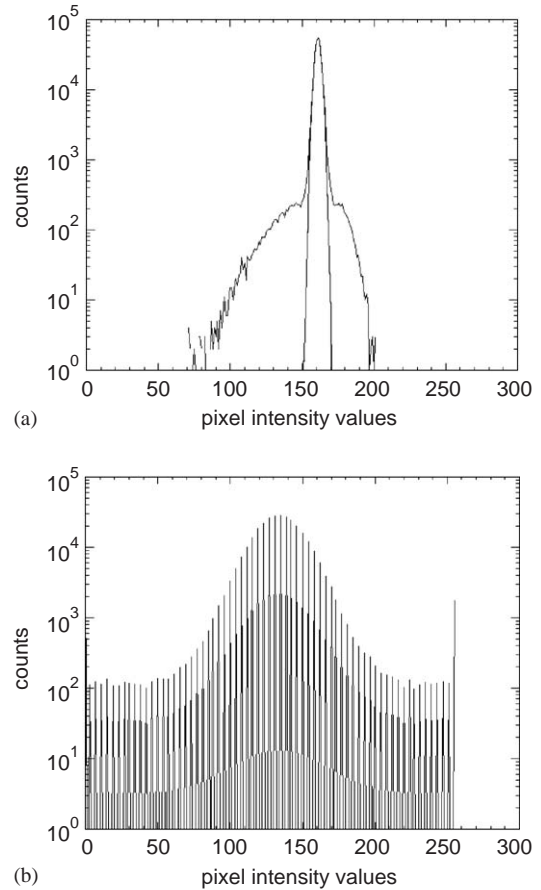


Fig. 2. Typical intensity histogram with Gaussian curve fit (a). Histogram of an image after contrast enhancement (b).

is that there is no general increasing trend in contrast towards totality (and decreasing trend afterwards) as usually had been observed. This can only be seen a few seconds before a second contact. This might be an atypical solar eclipse, as far as shadow bands are concerned.

Two operations that could be used to detect shadow bands are:

- computation of the cross-correlation between two successive images to demonstrate the movement of coherent pattern between frames,
- application of a FFT algorithm to a single image in order to find the shape of power spectral density function, $psd(k)$, defined by Kay and Marple (1981), as predicted by Codona, and search for shadow bands' characteristic spatial frequencies.

In the case of two images, the cross-correlation function is also an image that should have a bright

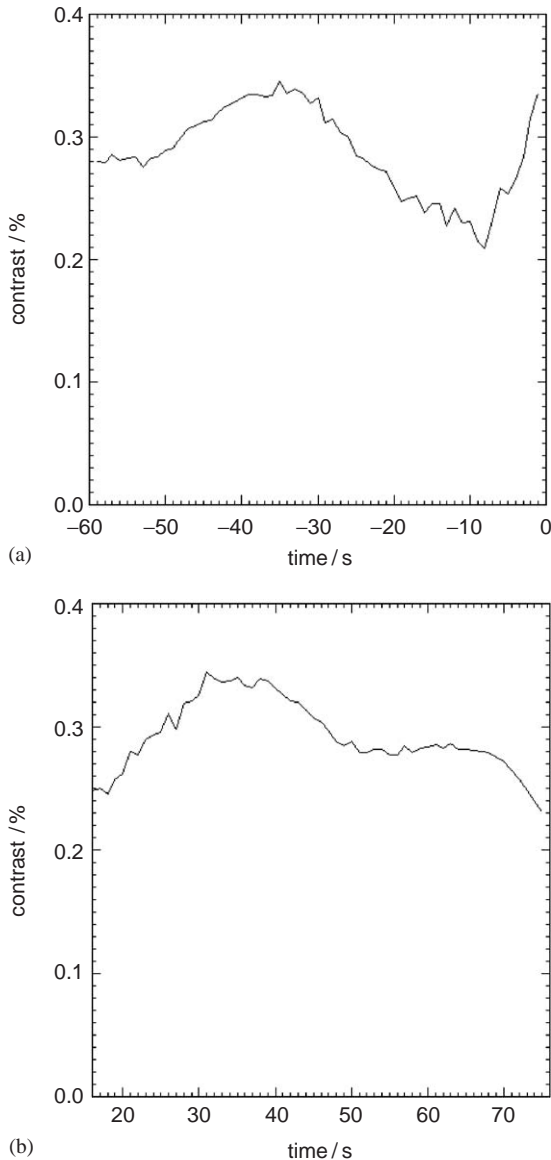


Fig. 3. Shadow band contrast before second contact (a) and after third contact (b).

peak with coordinates matching the relative movement of a coherent pattern—as long as there is, indeed, coherent movement between two frames. We wanted to determine if the images really show shadow bands by checking if cross-correlation yields the movement vector that corresponds to given wind speed and direction of the solar crescent (this vector would have a magnitude of around 40 pixels). Unfortunately that did not happen—cross-correlation for different pairs of raw (without contrast enhancement) images revealed nothing but a peak at (0,0) coordinates (Fig. 4). This means that the random variations in reflectivity of the screen (hardly

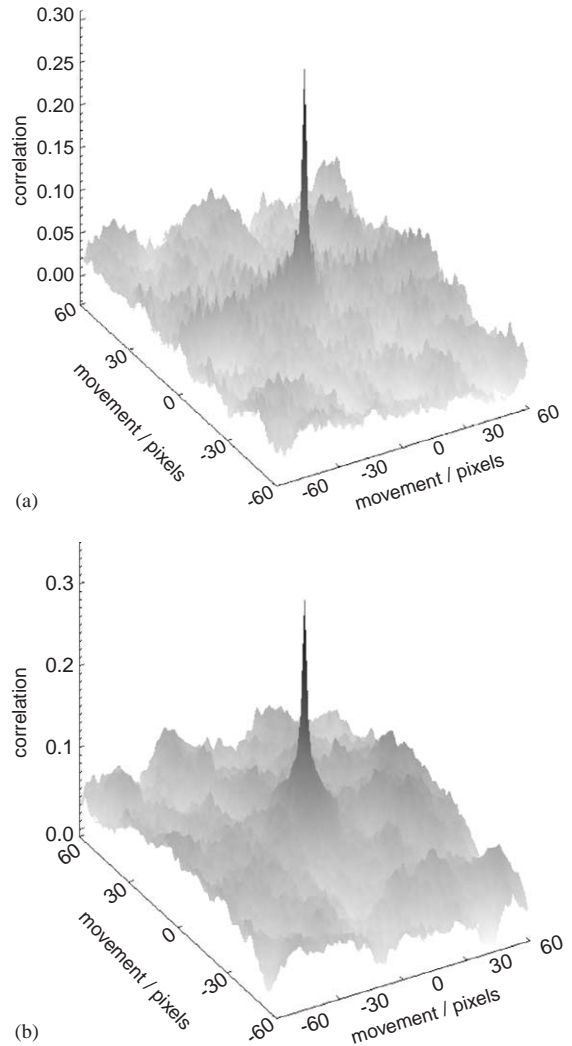


Fig. 4. Cross-correlation functions (shown here as surface plots) for two subsequent images before (a) and after (b) totality.

visible with an unaided eye) are more pronounced than the shadow bands—even after flat-fielding some artefacts remained. Besides that, 25 fps means 40 ms between frames, while Taylor's hypothesis predicts that the coherence time (t_0) for the atmosphere is approximately 10 ms ($\lambda = 500$ nm, wind speed ~ 10 m s $^{-1}$, spatial coherence, $r_0 = 10$ cm, Monnier, 2003). Recent measurements of t_0 (Davis, Tango, 1996) have yielded even smaller values which covered the range 1–7 ms. Shadow bands change their shape significantly from one image to the next—one would expect little cross-correlation between them.

Power spectral density functions were more likely to reveal shadow bands as they are calculated in the spatial domain so that low fps limit of the digital video recorder

played no role here. We recorded ambient noise at a low light level with the recorder (same settings as on the observation day, we used images with dimensions 620×490 pixels corresponding to 1000 and 800 mm), and calculated averaged and normalized noise *psd* for the resulting ensemble of images. The *psd* of an image is a two-dimensional function but for the purpose of this study a one-dimensional *psd* was calculated in order to make comparisons with Codona’s plots. First, the direction of the solar crescent had to be established: *psd*’s have to be calculated perpendicular to it as that is the direction of shadow bands’ spacing. ‘TheSky’ astronomy software was used to do this: with all the parameters of the eclipse given as input it generated a simulation of the Sun–Moon movement on the specified date. Power spectra for the pixel vectors at a right angle to the tangent to the crescent were calculated separately, added and averaged to produce a *psd(k)* plot. The *psd* of the noise (Fig. 5) was then subtracted from each *psd* of the shadow bands. Smoothing with a rectangular window, 4 pixels wide, was used. Sixty such functions were computed before and after totality, setting the interval between measurements to 1 s. Fig. 6 shows some of them. The cut-off frequency was imposed by the Nyquist theorem. In some cases noise cancelled the signal in the very low-frequency range, but that part of the plots was not significant for further analysis.

The qualitative resemblance between our power spectral density functions and the plot resulting from theoretical assumptions in Codona’s paper is striking. As expected the images from the range of highest contrast (40–30 s before, and 30–40 s after the total phase, Fig. 3) yielded most distinct shadow bands’ *psd*’s. The pattern disappears very close to totality and approximately 1 min after third contact (due to low

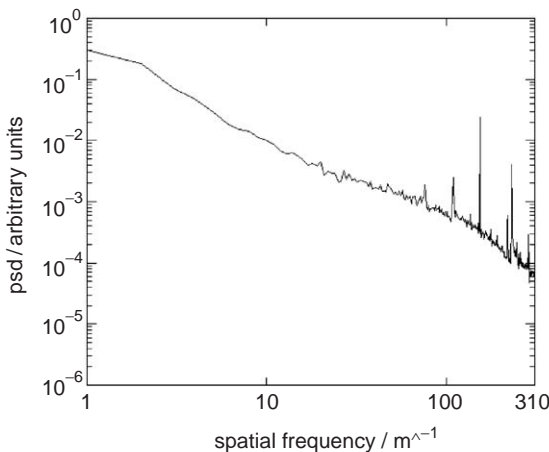


Fig. 5. Normalized power spectral density function of recorder’s noise. Both axes are logarithmic.

signal-to-noise ratio). In those *psd* plots in which the expected pattern of peaks is most pronounced, signal in the range of interest is an order of magnitude above the noise level. Apart from that, the *psd* of noise decreases almost linearly with frequency, so the characteristic oscillations of the atmospheric propagation together with slowly increasing or constant low-frequency content seen in the *psd*’s we recorded can be explained only by the presence of the shadow bands. According to Codona, shadow bands’ *psd*’s would display three characteristic scales. Which of them will be the dominant shadow band scale *visible to the human eye* would depend on the distance of the atmospheric scattering layer from the observer and the time to totality. First characteristic scale, L_{peak} , is controlled by the geometry of the crescent and corresponds to the low-frequency peak in the spectrum. The next scale, L_{source} relates to the first minimum in the plots and is due to the first null of the source’s spectrum. The third scale corresponds to the fast oscillating term in the analytic expression, introduced by the intensity spectrum of a plane wave incident on a weakly scattering thin phase-screen (scattering layer). These oscillations start at the second minimum in the plots.

In Codona’s thin turbulent layer theory, the higher frequency structure in the *psd*’s, particularly the first pronounced minimum, should be a few tens of times the frequency $1/L_{\text{peak}}$, whereas we see such a minimum at only about $2/L_{\text{peak}}$. It is likely that this is due to the distributed nature of the scattering, which in reality is not confined to a thin layer.

Codona derived formulae relating the height of the scattering layer z to the dominant spatial frequency of a *psd* plot. He gave special attention to the effects he called ‘smoky wisps’ (similar to a crude Schlieren camera). These are shadow bands produced by a scattering layer very near the observer (100 m or less). Visual studies on the day suggested that solar eclipse of 4 December 2002 generated this specific kind of phenomenon. Codona predicts that smoky wisps would be produced by eclipses with a small ϵ parameter ($\epsilon = r - 1$). According to him, typical values for ϵ are between 0 and 0.12. In the case of the Botswana eclipse, a value of only 0.018 indicates that the observed shadow bands were indeed caused by low-level scattering. At $t = 55$ s before second contact (totality onset, top left in Fig. 6), and using $L_{\text{peak}} = 0.029$ m ($1\text{ m}/10^{1.54}$, from Fig. 6), yields $z = 3.15$ m, indeed a very low altitude.

Use was made of the values of L_{source} instead. The respective formula for z is

$$z = \frac{L_{\text{source}}}{R_S \tau},$$

where R_S is the angular radius of the Sun and $\tau = \Omega |t - t_{\text{contact}}| / R_S$ is the normalised time away from

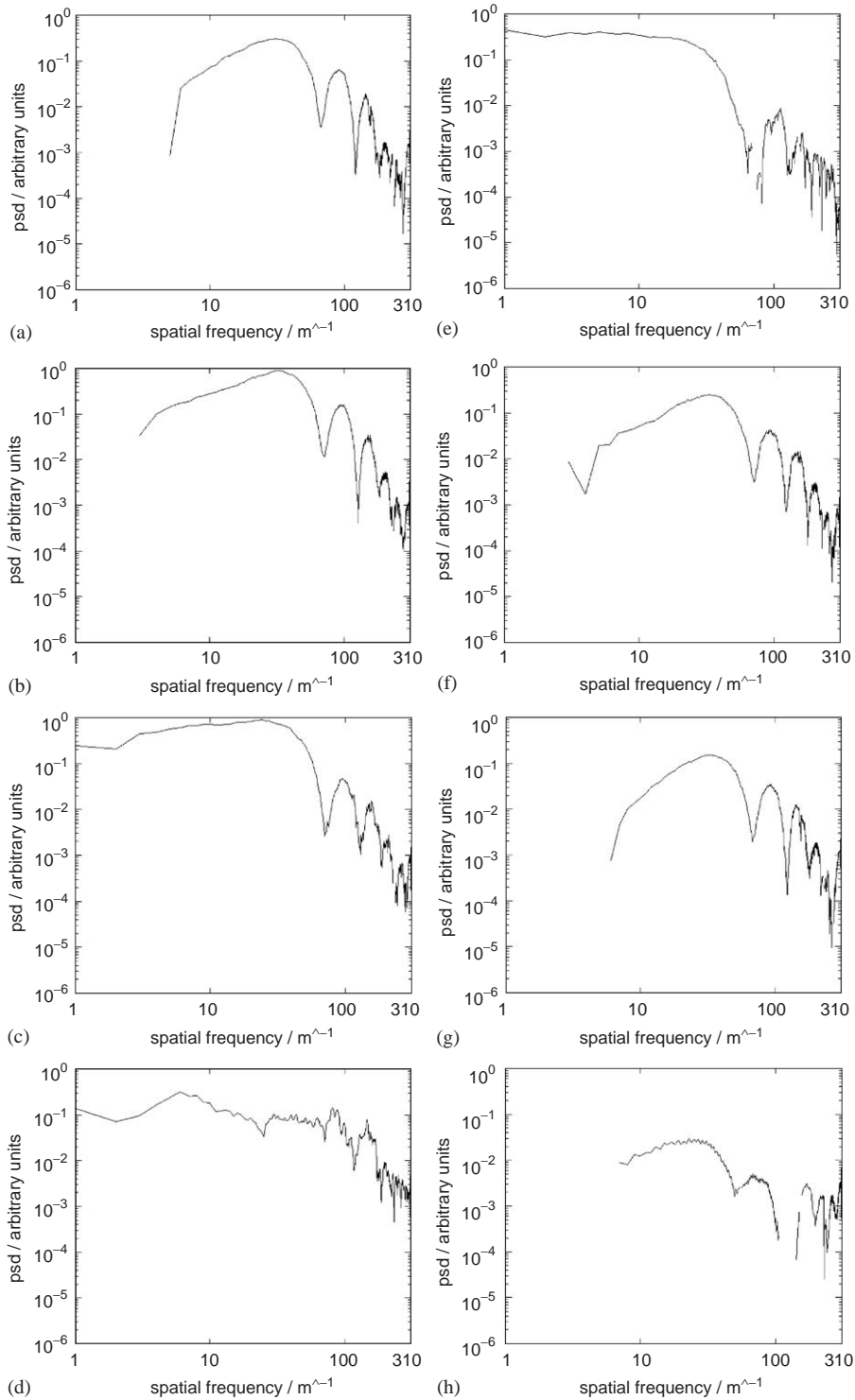


Fig. 6. De-noised and smoothed power spectral density functions for images 55 (a), 41 (b), 26 (c) and 8 (d) s before totality, and (on the right) 18 (e), 44 (f), 51 (g) and 69 (h) s after totality (logarithmic axes).

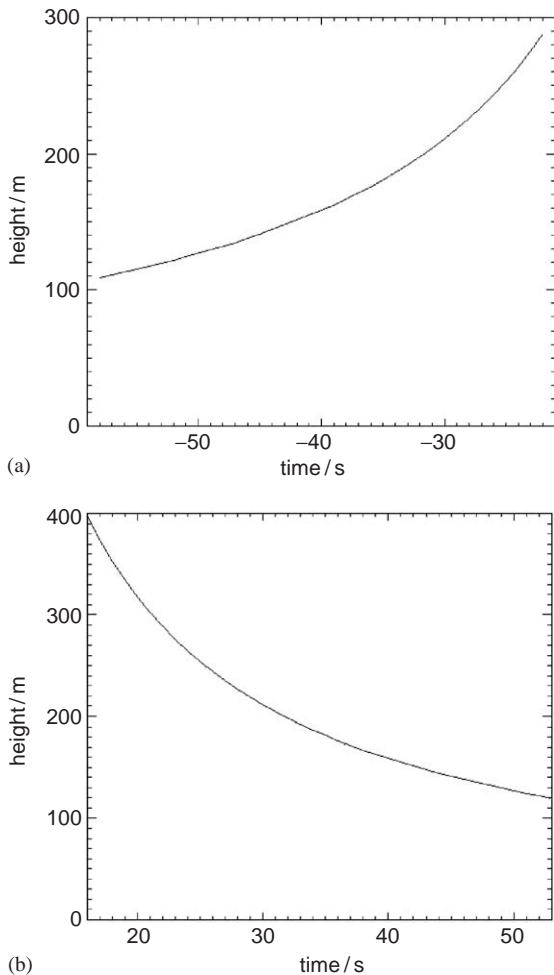


Fig. 7. Scattering layer's height before (a) and after (b) total phase.

totality, and t_{contact} is the time of either second or third contact (t being the time).

The most pronounced shadow bands' plots were chosen and their first minima extracted for further analysis. The values of the phenomenon's width, derived from the functions' minima, did not change with time significantly, so the average value of 0.014 m was assumed in further calculations. From the values of L_{source} it was possible to calculate the distance from the observer to the scattering layer. Again, only values corresponding to crisp shadow bands' psd 's are shown (Fig. 7).

The two plots are symmetrical and the range of values (z) is in agreement with previous observations (Jones, 1999).

5. Conclusions

This paper's aim is to present a new approach to recording and analyzing shadow bands. Images

obtained allowed spatial analysis for the first time. That created the opportunity to directly compare results with the theory which is mostly based in the spatial domain. Previous observations and comparisons to theory relied upon an approximate conversion to the spatio-temporal domain. Codona's theory assumes that the spatial power spectral density of the shadow bands arises from the incoherent thin crescent source, the solar eclipse crescent, illuminating a thin phase screen (use is made of the standard, weak scattering model). The shape of the resulting psd function is controlled by the geometry of the crescent and the atmospheric propagation model. Confirmation of the relevance of the theory was achieved. Power spectral density functions are in excellent agreement with the predicted shape.

In order to make fully quantitative comparisons with the theory it is necessary to have details of the extended atmospheric turbulence at the time when shadow bands are being recorded. These data were unavailable in Botswana. Future experiments will hopefully incorporate fast digital recorders and equipment to measure the C_n^2 profile during the brief interval of totality (Tokovinin and Kornilov, 2002). This will allow detection of shadow bands' movement (via cross-correlation of images), and fully reliable results regarding scattering layers could be produced. During the next convenient total solar eclipse (in North Africa, 29 March 2006), it is our aim to obtain high fps recording and C_n^2 data.

Acknowledgments

SG was funded by CosmoGrid project (Grid-enabled Computational Physics of Natural Phenomena). The authors would like to thank Thierry Daubos of NUI Galway for his introduction to IDL programming language and many useful thought-provoking discussions.

References

- Codona, C., 1986. The scintillation theory of eclipse shadow bands. *Astronomy and Astrophysics* 164, 415–427.
- Davis, J., Tango, W.J., 1996. Measurement of the atmospheric coherence time. *Publications of the Astronomical Society of the Pacific* 108, 456–458.
- Esenak, F., Anderson, J., 2001. Total solar eclipse of 2002 December 4. *NASA Eclipse Bulletin*, TP 2001-209990.
- Glasbey, C.A., Mardia, K.V., 1998. A review of image warping methods. *Journal of Applied Statistics* 25, 155–171.
- Jones, B.W., 1996. Shadow bands during the total solar eclipse of 3 November 1994. *Journal of Atmospheric and Terrestrial Physics* 58, 1309–1316.
- Jones, B.W., 1999. Shadow bands during the total solar eclipse of 26 February 1998. *Journal of Atmospheric and Solar-Terrestrial Physics* 61, 965–974.

- Jones, B.W., Jones, C.A.L., 1996. Shadow bands during the total solar eclipse of 11 July 1991. *Journal of Atmospheric and Terrestrial Physics* 56, 1535–1543.
- Kay, S.M., Marple, S.L., 1981. Spectrum analysis—a modern perspective. *Proceedings of the IEEE* 69, 1380–1419.
- Lindler, D., Bohlin, R., Hartig, G., Keyes, C., 1993. FOS flats from super spectra. FOS Instrument Science Report CAL/FOS-088
- Marschall, L.A., Mahon, R., Henry, R.C., 1984. Observations of shadow bands at the total solar eclipse of 16 February 1980. *Applied Optics* 23, 4390–4393.
- Monnier, J.D., 2003. Optical interferometry in astronomy. *Reports on Progress in Physics* 66, 789–857.
- Tokovinin, A., Kornilov, V., 2002. Measuring turbulence profile from scintillations of single stars. Astronomical site evaluation in the visible and radio range. *ASP Conference Proceedings* 266, 104–111.